

Prior-based artifact correction for clinical and for flat detector CT

Poster No.: C-1870
Congress: ECR 2013
Type: Scientific Exhibit
Authors: T. Heußer¹, M. Brehm², S. Sawall², M. Kachelrieß¹; ¹Heidelberg/DE, ²Erlangen/DE
Keywords: Radiation physics, CT, Physics, Artifacts
DOI: 10.1594/ecr2013/C-1870

Any information contained in this pdf file is automatically generated from digital material submitted to EPOS by third parties in the form of scientific presentations. References to any names, marks, products, or services of third parties or hypertext links to third-party sites or information are provided solely as a convenience to you and do not in any way constitute or imply ECR's endorsement, sponsorship or recommendation of the third party, information, product or service. ECR is not responsible for the content of these pages and does not make any representations regarding the content or accuracy of material in this file.

As per copyright regulations, any unauthorised use of the material or parts thereof as well as commercial reproduction or multiple distribution by any traditional or electronically based reproduction/publication method ist strictly prohibited.

You agree to defend, indemnify, and hold ECR harmless from and against any and all claims, damages, costs, and expenses, including attorneys' fees, arising from or related to your use of these pages.

Please note: Links to movies, ppt slideshows and any other multimedia files are not available in the pdf version of presentations.

www.myESR.org

Purpose

Image quality in x-ray CT often suffers from artifacts due to missing data. In clinical CT for example, severe artifacts arise when metal objects, e.g. metal hip implants or metal pedicle screws, are present in the patient body. In flat detector CT additional artifacts originate from projection truncation, which occurs when the patient is larger than the field of measurement covered by the detector. Other artifacts result from a limited scan angle when the CT device cannot perform a full 180° rotation, for example in some interventional C-arm CT devices. Examples for metal and truncation artifacts are presented in [Fig. 1](#) on page 3.

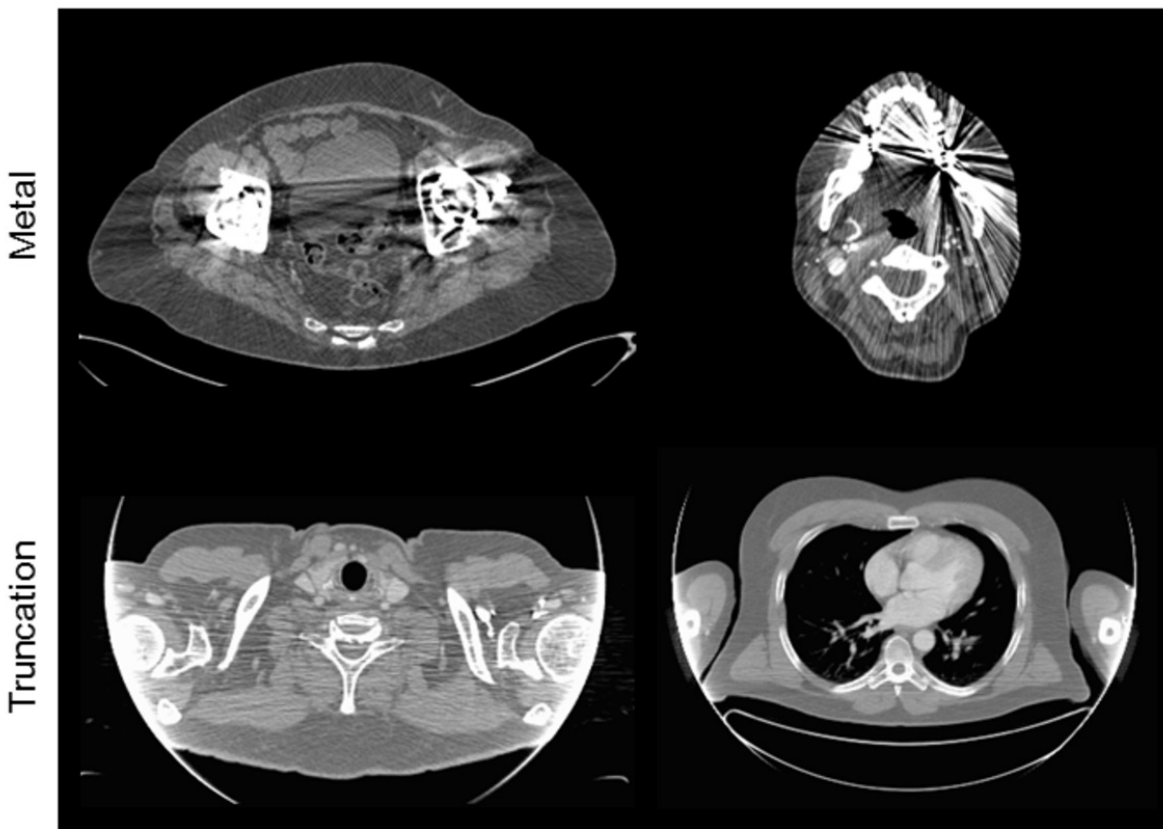


Fig. 1: Typical cases showing the occurrences of metal (top row) and truncation (bottom row) artifacts.

References: Medical Physics in Radiology, German Cancer Research Center (DKFZ) - Heidelberg/DE

Many techniques to correct for these artifacts can be found in the literature. For metal artifacts, most common is the inpainting technique where the measured data inside

the metal trace are declared to be untrustworthy and therefore have to be replaced by appropriate surrogate data. A variety of methods to determine these surrogate data has been proposed [1-5]. There are some but by far not as many publications dealing with a limited angular scan range [6-8]. A promising approach is based on the compressive sensing framework. In case of truncated data, most investigations perform data extrapolation to allow for a smooth transition from the measured data to zero [9-11].

The existing correction techniques are specific for each type of artifact and, to our knowledge, there is no work that studies the effects of combining several of these artifact correction methods. In many cases, the existing methods struggle with completely removing the artifacts while not introducing new artifacts at the same time. However, prior data is available in many cases which can, potentially, be used to correct for the missing data.

The aim of this work is to introduce a generalized prior-based artifact correction (PBAC) method for prominent CT artifacts resulting from missing data by performing data completion based on prior knowledge. The prior data may be taken from a planning CT of the same patient, if available, or from a patient database. These artifact-free prior data are matched to the measured patient data using a non-rigid registration algorithm, followed by forward projection, smooth sinogram inpainting, and image reconstruction. The corrected images using PBAC are compared to the corresponding ground truth and to results obtained with conventional artifact correction methods.

Images for this section:

Metal

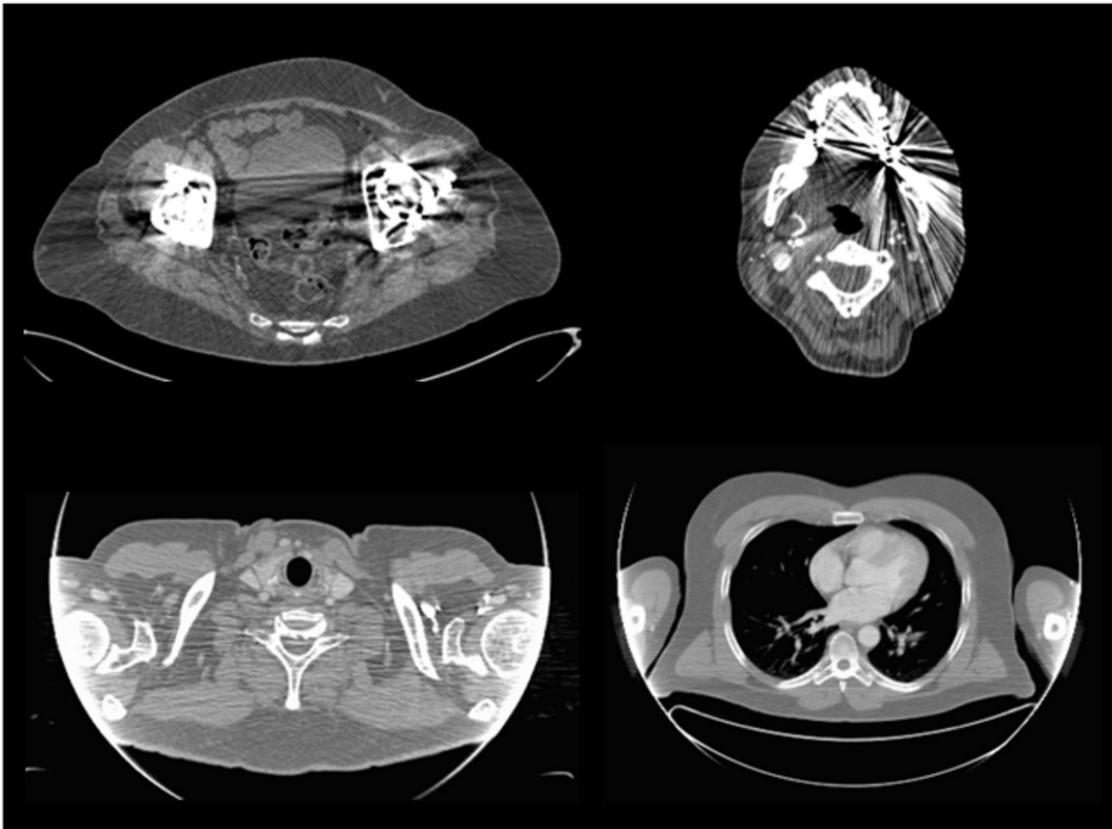


Fig. 1: Typical cases showing the occurrences of metal (top row) and truncation (bottom row) artifacts.

Methods and Materials

Artifact Simulation

The prior-based artifact correction (PBAC) method is evaluated using several patient datasets containing simulated missing data regions. We chose to simulate missing data regions by modifying the measured projection data rather than to use real incomplete scans in order to allow for a comparison against the ground truth. All experiments were conducted using 3D volumetric data sets measured at clinical CT scanners at the German Cancer Research Center (DKFZ), Heidelberg, Germany. The slices presented in this work are referred to as images nonetheless.

Representative slices of the reconstructions before (ground truth) and after (uncorrected images) the modifications in the projection data to simulate the missing data regions are presented in [Fig. 2](#) on page 11.

To simulate metal artifacts, two artificial metal pedicle screws are included in the projection data belonging to the thorax scan. The projection values of these metal screws are computed considering polychromatic attenuation and are added onto the measured projection data.

By reducing the size of the detector such that the patient is not completely enclosed in the field of measurement (FOM) anymore, truncated data is simulated for a hip dataset. The FOM, indicated by the red circle in [Fig. 2](#) on page 11, is reduced from 79 cm to 39 cm due to the smaller detector.

Finally, artifacts due to a limited angle scan are simulated for a head scan by reducing the angular range from $180^\circ + \#$ to $120^\circ + \#$ with $\#$ being the fan angle. The CT values are weighted accordingly. In [Fig. 2](#) on page 11, the trajectory of the source is illustrated by the red arc.

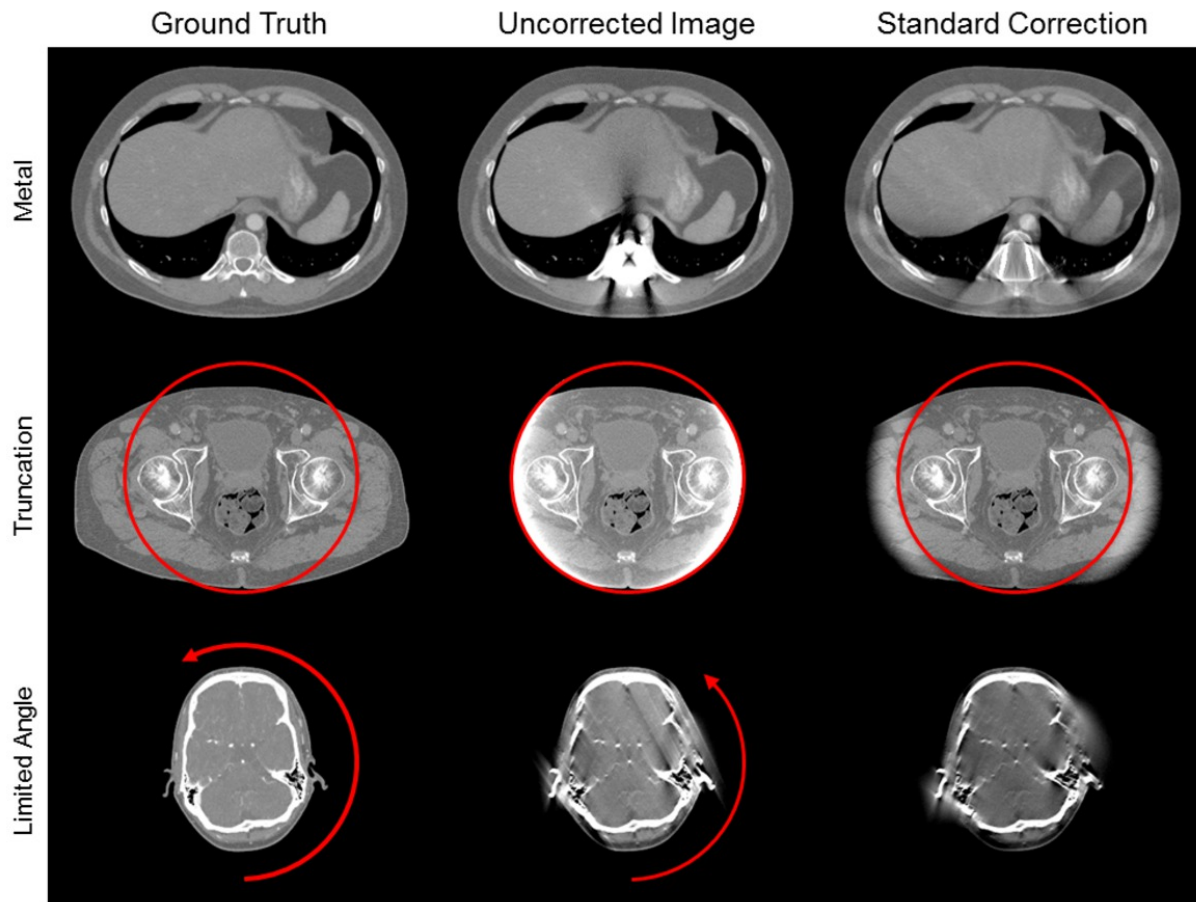


Fig. 2: Ground truths, uncorrected images, and standard corrections for the different types of artifacts investigated in this work. In the truncation case, the reduced FOM is indicated by the red circle. The red arc illustrates the trajectory of the source in the limited angle case. $C = 0$ HU, $W = 1000$ HU.

References: Medical Physics in Radiology, German Cancer Research Center (DKFZ) - Heidelberg/DE

Standard Correction

For each of the artifacts described above a conventional correction method using data extrapolation or interpolation is performed. These methods are specific for each type of artifact and will be referred to as standard corrections in the following.

The metal artifacts are corrected by using linear interpolation between the boundaries of the metal in the projection data. The metal itself is segmented by simple thresholding in the uncorrected image and incorporated into the corrected image by replacing the corresponding pixels. In case of truncated data, a detector enlargement followed by a smooth \cos^2 -extrapolation of the measured data to zero is used to correct for the artifacts.

The standard correction for limited angle artifacts is a smooth outfading of the projection values in angular direction. Results of the standard corrections are shown in the right column of [Fig. 2](#) on page 11.

Data Completion Method

The flowchart presented in [Fig. 3](#) on page 11 illustrates the proposed data completion approach by showing the correction of metal artifacts in a thorax scan as an example. Despite the simplified illustration of the metal case, the basic principle of the method is applicable to other artifacts, e.g., truncation artifacts and artifacts due to a limited scan angle. In the following a general description is given how PBAC is performed.

Let us start with incomplete and thereby inconsistent projection data p . A standard reconstruction of p yields an image or a volume f containing some of the previously mentioned artifacts that need to be corrected for. With X denoting the x-ray transform we have X^{-1} denoting image reconstruction, which in many cases is a conventional 2D filtered backprojection algorithm or, like in the work presented here, a 3D filtered backprojection based on the Feldkamp algorithm of reference [12]. In the following, we assume the entries of p to be set to zero for those rays which correspond to missing data. In the metal case, the projection data corresponding to the metal trace are discarded and set to zero.

Using the notation of reference [13] we decompose the x-ray transform into measured and unmeasured rays $X = X_M + X_U$, with the latter corresponding to the missing data that shall be completed.

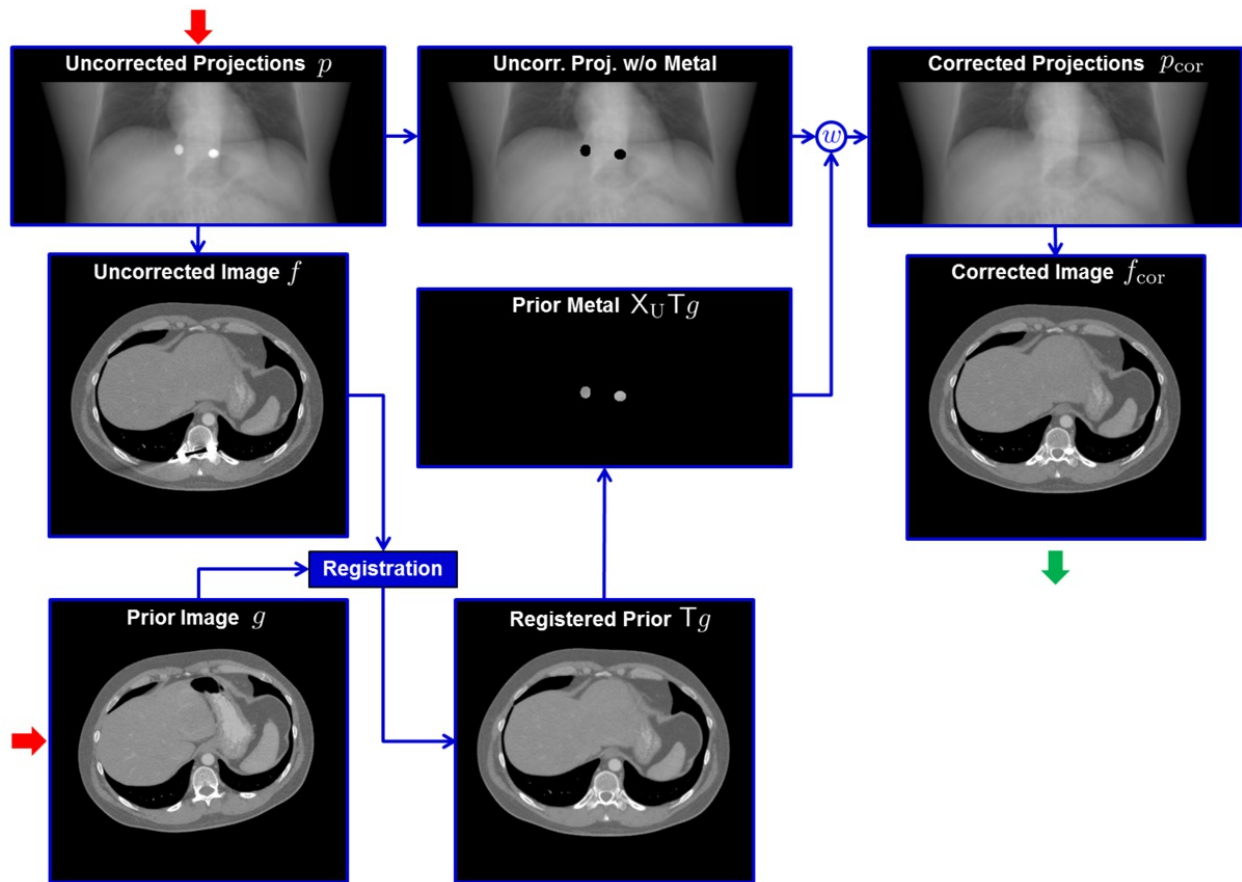


Fig. 3: Flowchart of the proposed prior-based artifact correction (PBAC) showing the correction of metal artifacts in a thorax scan as an example. Input data are marked with red arrows, while the output of the algorithm is indicated by the green arrow.

References: Medical Physics in Radiology, German Cancer Research Center (DKFZ) - Heidelberg/DE

Let the prior image g be a nearly artifact-free CT image of the same patient or from a patient database. This prior image g is registered to the uncorrected image f to obtain an artifact-free image Tg that is similar to f . The registration process, described by T , can be a rigid or a non-rigid transformation. The image Tg is forward projected in the geometry of the uncorrected projections p using Joseph's algorithm [14]. The forward projection is done only along those rays that are missing, plus a small overlap zone to allow for a smooth transition between the measured and the incorporated data. The smooth transition is ensured by including a weighting factor w . Hence, we obtain $X_U Tg$ which we use to fill in the missing regions in p and to compute the corrected projections $p_{cor} = p + w \cdot (X_U Tg)$.

The corrected projections p_{cor} can now be used for image reconstruction. This finally results in the corrected image $f_{cor} = X^{-1} p_{cor}$.

Prior Data and Registration

To perform PBAC adequate prior data are needed. The prior data used in this work were measured using the same clinical CT scanners as for the patient data. Prior data taken from a different scan of the same patient or from a scan of a different patient are used.

Before the prior information can be incorporated into the missing data regions to perform data completion the prior image g has to be co-registered with the uncorrected image f . This is necessary to compensate for differences between acquisitions due to a changed patient positioning or between two actual patients.

In this work, the registration process consists of two steps. First, an affine registration corrects principle parts of the misalignment between the two images which are to be aligned. The affine registration allows for scaling and translation in all three spatial dimensions as well as for a rotation around an arbitrary rotation axis. We use the normalized mutual information [15,16] as measure of similarity between f and g during our experiments. The maximization of the similarity criterion is done by a genetic algorithm [17] ensuring that a global optimum is found.

However, the results in Fig. 4 on page 12 show that the anatomical differences between the two different thorax patients co-registered here cannot be compensated by the affine transformation. This is also true for two scans of the same patient where differences due to the acquisition in different respiratory phases cannot be sufficiently corrected for by using an affine registration.

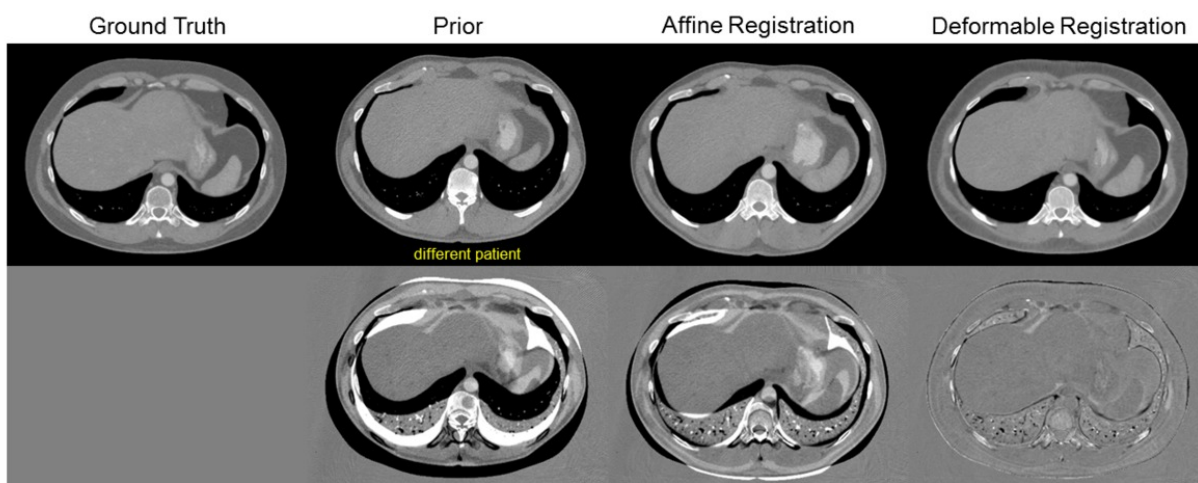


Fig. 4: Results of the affine and the subsequent deformable registration. The difference images show the difference to the ground truth. $C = 0$ HU, $W = 1000$ HU for reconstructions and for difference images.

References: Medical Physics in Radiology, German Cancer Research Center (DKFZ) - Heidelberg/DE

Therefore, as a second step, a deformable registration is performed to obtain more accurate results better suited for PBAC. The algorithm used in this work is based on reference [18]. The non-rigid registration allows for a local, voxel-specific deformation, in contrast to the global affine transformation. Results of the deformable registration are also found in Fig. 4 on page 12. It can clearly be seen that only small differences to the ground truth are left. This means, the deformable registration, in contrast to the affine transformation, is able to change the anatomy of the prior such that it matches the anatomy of the patient. It therefore provides appropriate surrogate data needed for data completion.

Data Visualization

For the radiologist it is important to know the impact of the prior image on the corrected image obtained by PBAC. He wants to know whether or not a pixel in the corrected image is influenced by the prior data which were used for data completion. The method proposed here makes use of the uncorrected and the corrected image only and explicitly does not require knowledge about the ground truth. Pixels influenced by the prior data are colored red with the intensity of the red color corresponding to the strength of the prior data influence.

To visualize the influence of the prior data on the corrected image f_{cor} we use the HSV color space. The hue H is set to $H = 0.0$, representing the color red. The value V is defined by the equation $V = f_{\text{cor}} \cdot s + l$.

where the slope s and the intercept l normalize V to the range $[0,1]$. The saturation S is computed by

$$S = \begin{cases} \Delta f & \text{if } \Delta f < t \\ t & \text{otherwise} \end{cases}$$

$$\text{where } \Delta f = \left| \frac{f_{\text{cor}} - f}{f_{\text{cor}}} \right|$$

$$\text{and } t \in [0, 1].$$

Fig. 5

References: Medical Physics in Radiology, German Cancer Research Center (DKFZ) - Heidelberg/DE

f is the normalized difference image between the corrected image f_{cor} and the uncorrected image f and t is a threshold. S is additionally smoothed by a Gaussian filter with FWHM = 9.4 mm.

Images for this section:

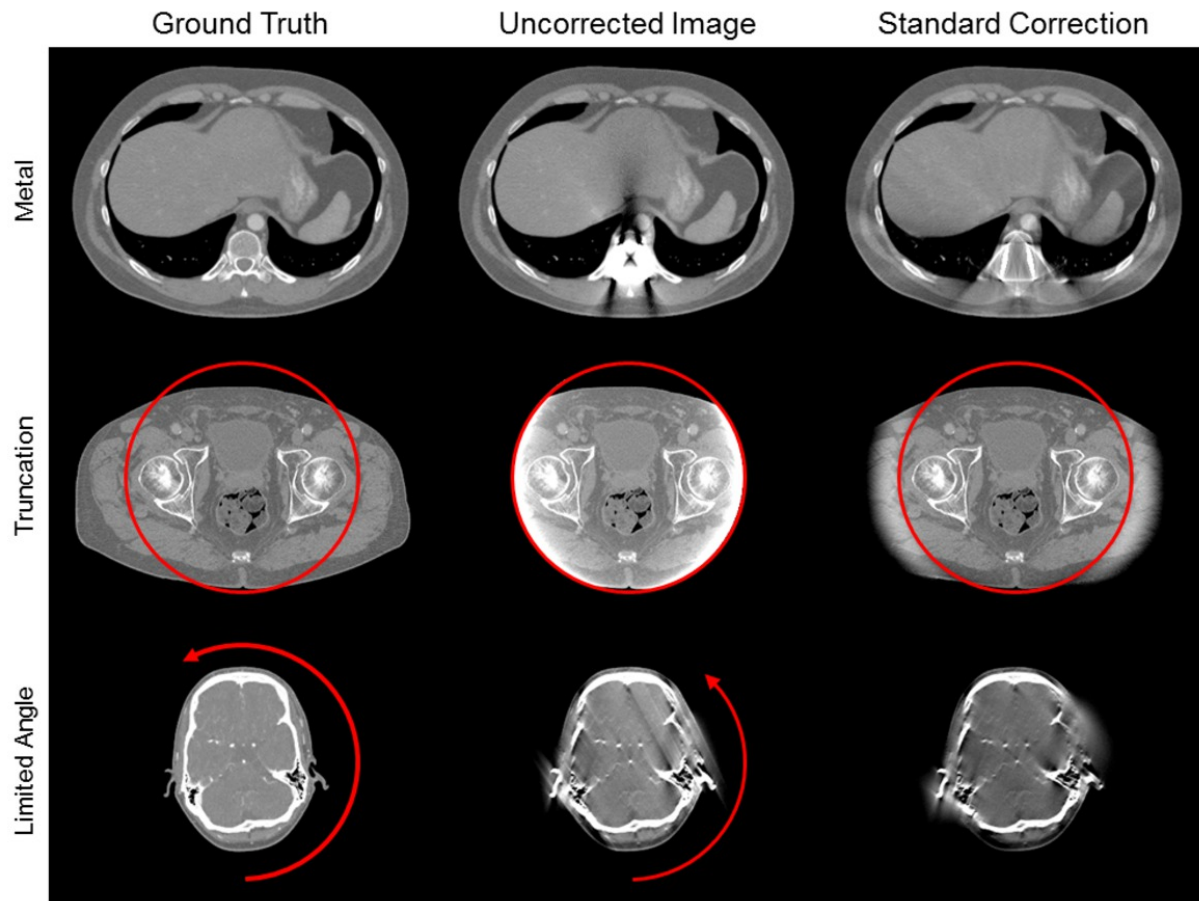


Fig. 2: Ground truths, uncorrected images, and standard corrections for the different types of artifacts investigated in this work. In the truncation case, the reduced FOM is indicated by the red circle. The red arc illustrates the trajectory of the source in the limited angle case. $C = 0$ HU, $W = 1000$ HU.

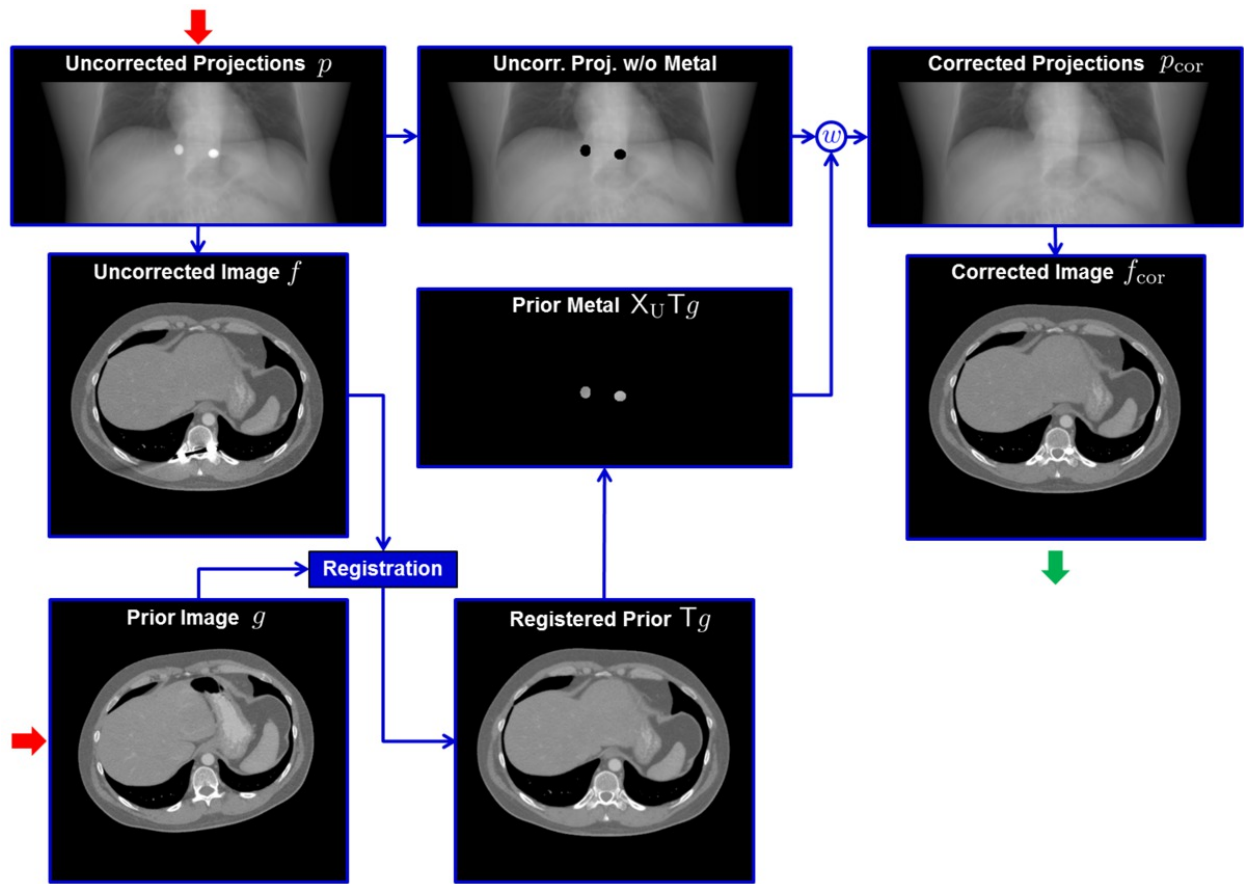


Fig. 3: Flowchart of the proposed prior-based artifact correction (PBAC) showing the correction of metal artifacts in a thorax scan as an example. Input data are marked with red arrows, while the output of the algorithm is indicated by the green arrow.

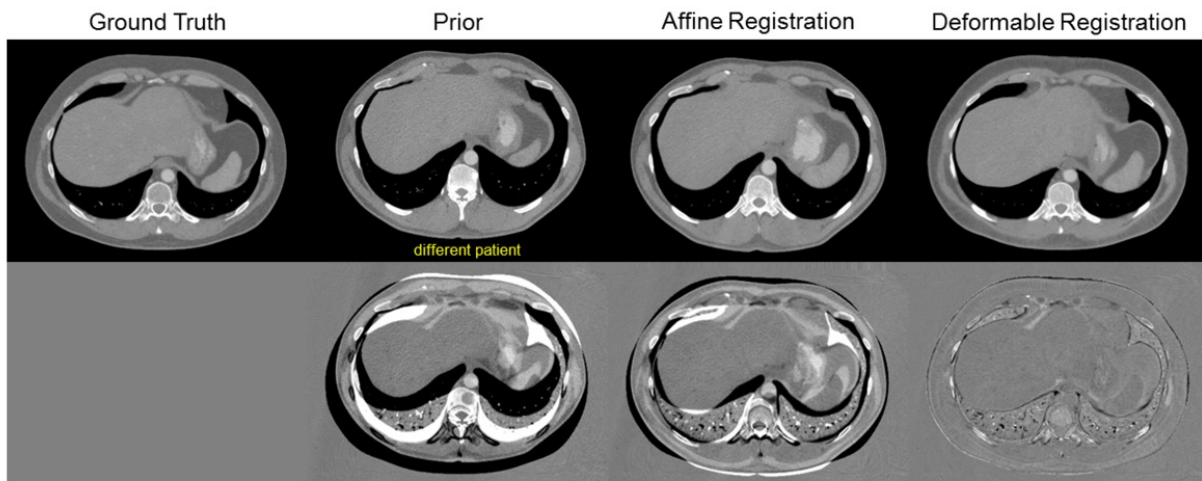


Fig. 4: Results of the affine and the subsequent deformable registration. The difference images show the difference to the ground truth. $C = 0$ HU, $W = 1000$ HU for reconstructions and for difference images.

Results

The results obtained with PBAC are compared to the corresponding ground truth, which serves as a benchmark, and to the corrected images obtained using the standard correction methods.

Metal Artifacts

Fig. 6 on page 18 shows the results in the case of metal artifacts. The top row includes the uncorrected image, the prior image used to perform data completion, the deformed prior after registration, and the corrected image obtained by PBAC. For a comparison, the corrected image using the standard correction method, i.e. linear interpolation, is also shown. On the bottom row, the corresponding ground truth (GT) is shown and the difference images to the GT are presented. It can clearly be seen that the corrected image obtained by PBAC is almost identical to the ground truth. The difference image shows that only minor streak artifacts remain. Compared to the standard correction method, PBAC achieves much better artifacts suppression while there is no visible degradation of bone structures in the vicinity of the inserted metal.

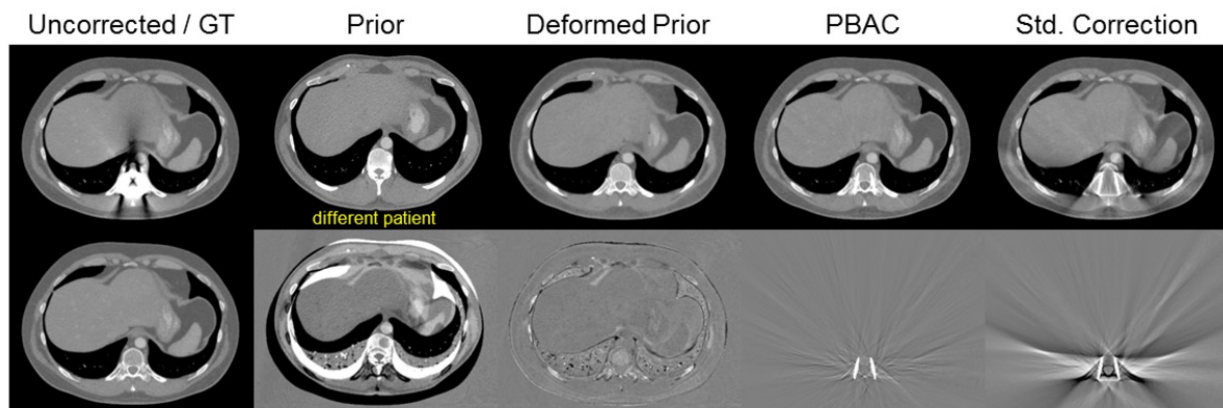


Fig. 6: PBAC results in the metal case. Top row: Uncorrected image, prior used for data completion, deformed prior after registration and the correction result obtained by PBAC. For a comparison, the standard correction is also shown. Bottom row: Ground truth (GT) and the corresponding difference images. $C = 0$ HU, $W = 1000$ HU for reconstructions and for difference images.

References: Medical Physics in Radiology, German Cancer Research Center (DKFZ) - Heidelberg/DE

Truncation Artifacts

The results for the truncation case are presented by Fig. 7 on page 18. The prior data used to perform data completion is taken from a scan of a different patient. For both PBAC and the standard correction method performing \cos^2 -extrapolation there is almost no difference to the GT within the reduced FOM. However, PBAC achieves even better suppression of the cupping artifacts.

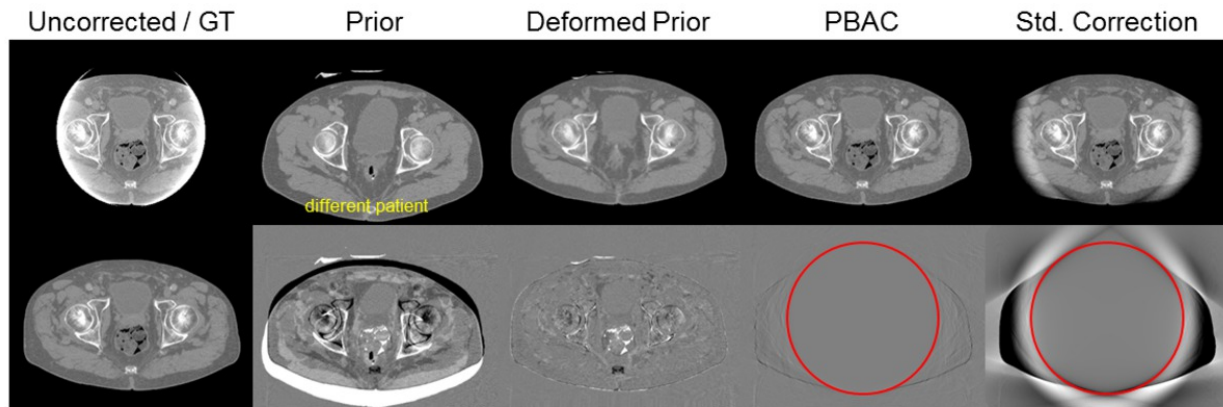


Fig. 7: PBAC results in the truncation case. Top row: Uncorrected image, prior used for data completion, deformed prior after registration and the correction result obtained by PBAC. For a comparison, the standard correction is also shown. Bottom row: Ground truth (GT) and the corresponding difference images. $C = 0$ HU, $W = 1000$ HU for reconstructions and for difference images.

References: Medical Physics in Radiology, German Cancer Research Center (DKFZ) - Heidelberg/DE

Limited Angle Artifacts

For the limited angle artifacts, the standard correction by angular outfading of the projection values reduces the streak artifacts but further increases the degradation of bone and other tissue. After PBAC, there are also artifacts left in the corrected image. Compared to the standard correction method however, the artifact suppression is greatly improved. There is no degradation of the patients' anatomy. The benefits of using PBAC to correct for limited angle artifacts are especially illustrated by the corresponding difference images in Fig. 8 on page 19.

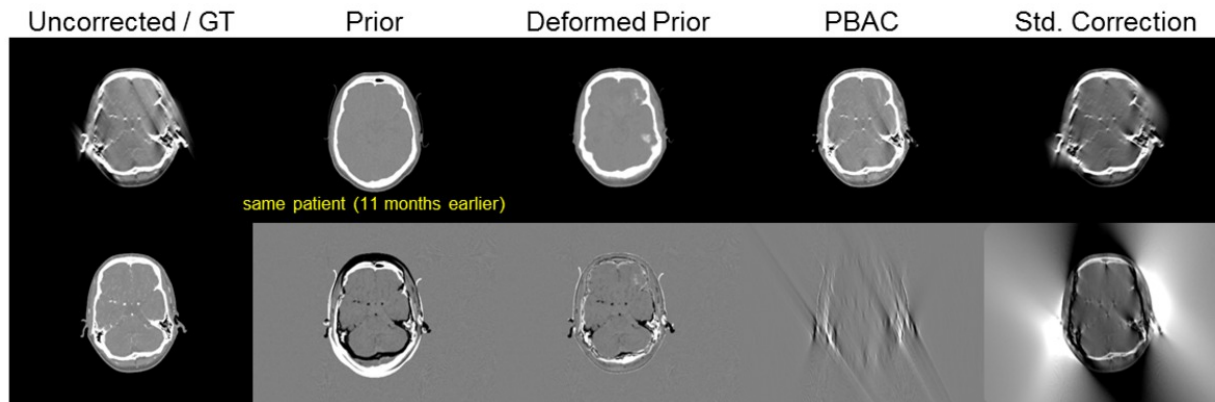


Fig. 8: PBAC results in the limited angle case. Top row: Uncorrected image, prior used for data completion, deformed prior after registration and the correction result obtained by PBAC. For a comparison, the standard correction is also shown. Bottom row: Ground truth (GT) and the corresponding difference images. $C = 0$ HU, $W = 1000$ HU for reconstructions and for difference images.

References: Medical Physics in Radiology, German Cancer Research Center (DKFZ) - Heidelberg/DE

Impact of the Prior Data

The uncorrected images and the corrected images obtained by PBAC and using the data visualization described in the methods and materials section are presented in [Fig. 9](#) on page 19. Pixels influenced by the prior data are colored red and therefore can immediately be identified. This way, an effective visualization of the prior data impact on the corrected image is provided to the radiologist. In the metal and in the truncation case, the prior data impact is limited to some parts of the corrected image. For limited angle artifacts however, the influence of the prior data on the corrected image is spread across the entire image. As mentioned above, the intensity of the red color correlates with the strength of the prior data influence.

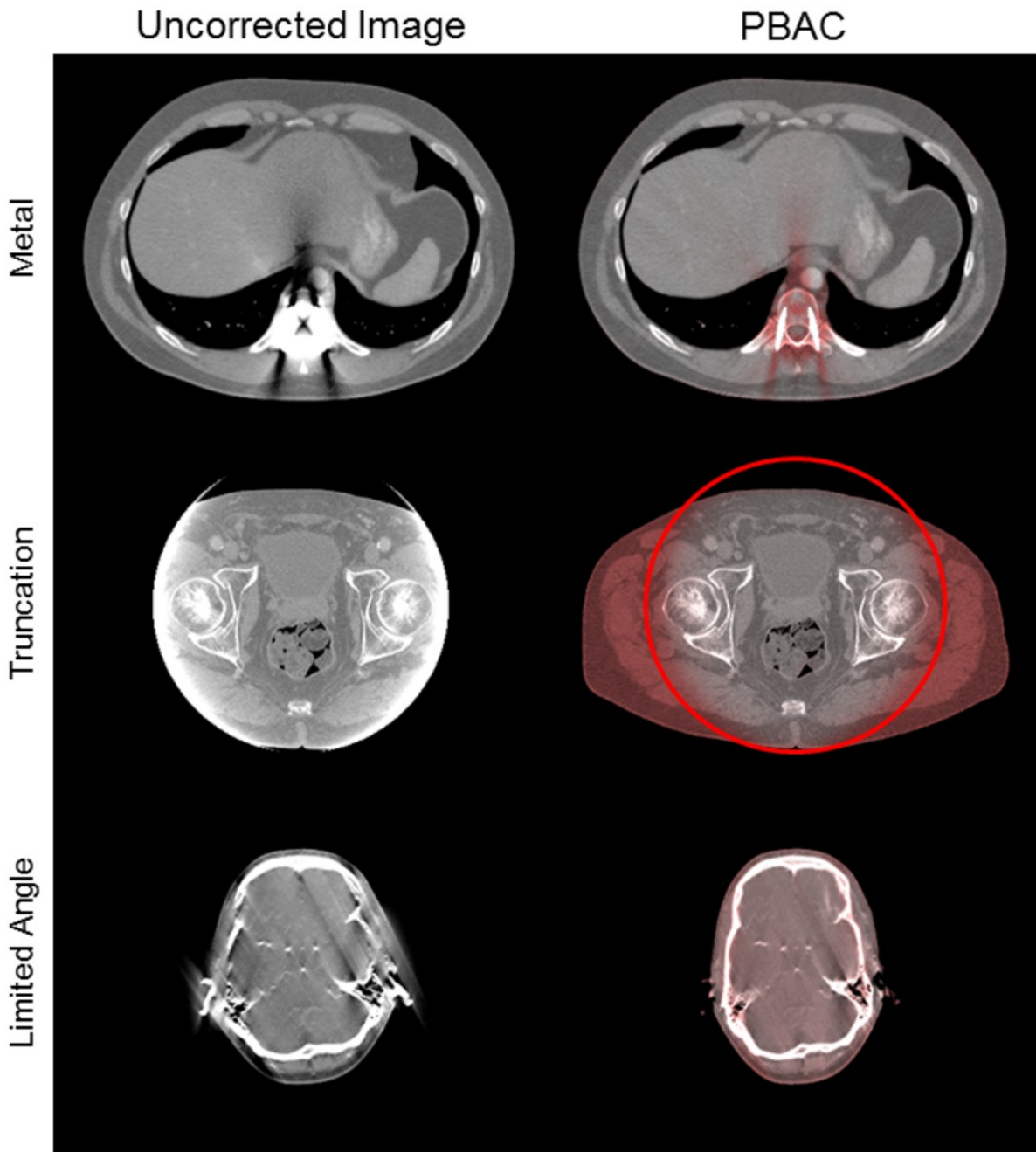


Fig. 9: Uncorrected and corrected images obtained by PBAC. The influence of the prior data is indicated by the red color. $C = 0$ HU, $W = 1000$ HU.

References: Medical Physics in Radiology, German Cancer Research Center (DKFZ) - Heidelberg/DE

It should be noted that although the red color indicates the pixels influenced by the prior data, it does not tell the radiologist whether these data truthfully represent the patient anatomy. PBAC aims in correcting for artifacts due to missing data without changing the original patients' anatomy. Therefore, the propagation of prior-specific information into

the corrected image is to be minimized. We investigate a situation where the prior is equal to the patient GT but includes some distinct anatomical details not present in the patient. These are two artificial structures in form of the DKFZ logo, one with a contrast of 50 HU and the other one with a contrast of 500 HU to the surrounding tissue. Results for PBAC are shown in Fig. 10 on page 20 for the metal case and in Fig. 11 on page 21 for the limited angle case.

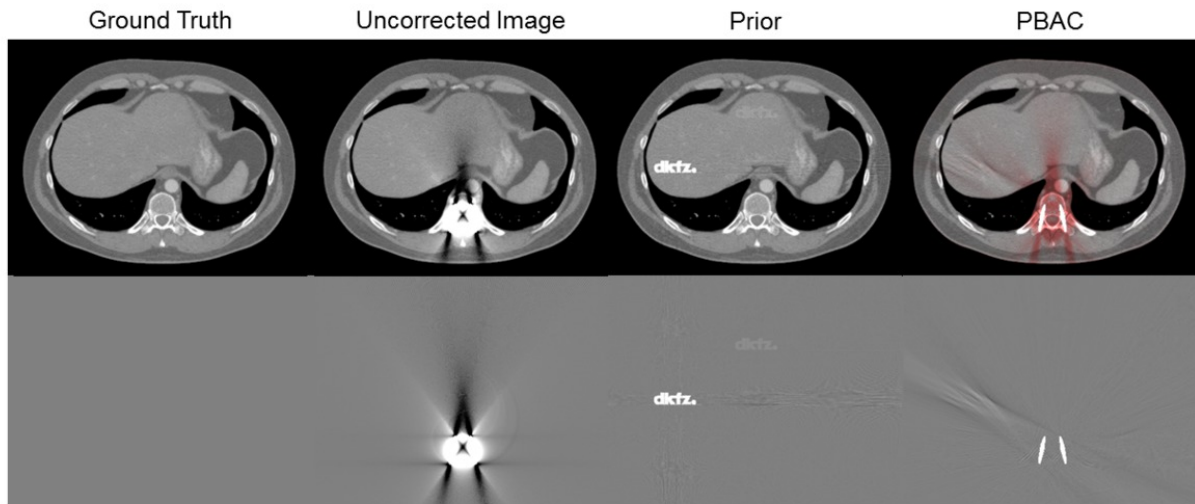


Fig. 10: Thorax patient with metal artifacts and the correction result obtained by performing PBAC using the ground truth including two artificial structures in form of the DKFZ-logo as prior. The difference images show the differences to the ground truth. $C = 0$ HU, $W = 1000$ HU for reconstructions and for difference images.

References: Medical Physics in Radiology, German Cancer Research Center (DKFZ) - Heidelberg/DE

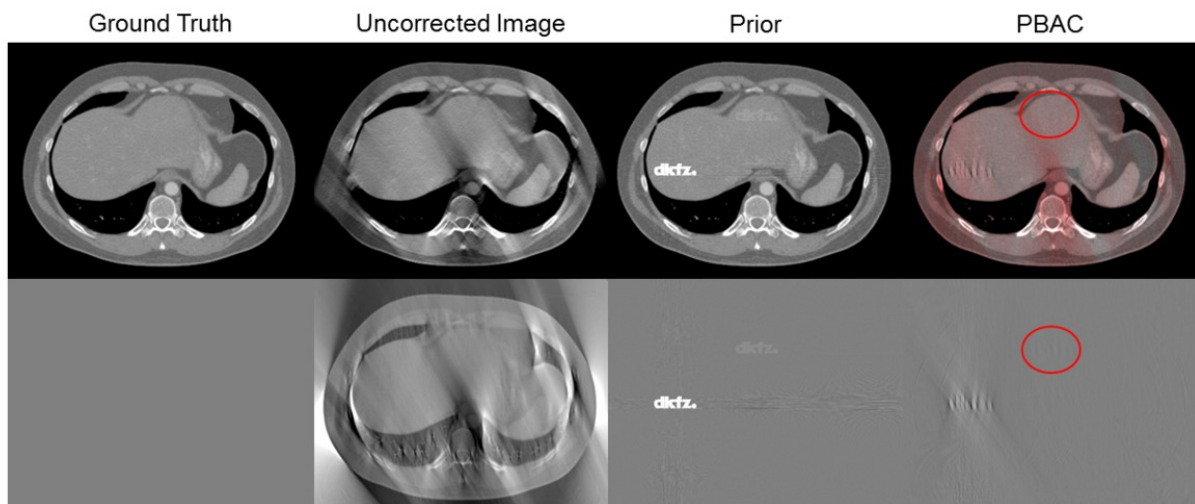


Fig. 11: Thorax patient with limited angle artifacts and the correction result obtained by performing PBAC using the ground truth including two artificial structures in form of the

DKFZ-logo as prior. The difference images show the differences to the ground truth. $C = 0$ HU, $W = 1000$ HU for reconstructions and for difference images.

References: Medical Physics in Radiology, German Cancer Research Center (DKFZ) - Heidelberg/DE

In the metal case, there obviously is some small impact of the 500 HU contrast logo onto the corrected image. An influence of the 50 HU contrast logo however is neither visible in the reconstructed image itself nor in the corresponding difference image. A greater impact of these artificial structures is found in the limited angle case. Here, the influence of the 500 HU contrast logo is clearly visible in both the corrected image and the corresponding difference image to the GT. A marginal influence of the 50 HU contrast logo, enclosed in the red oval, can also be seen in both images.

Images for this section:

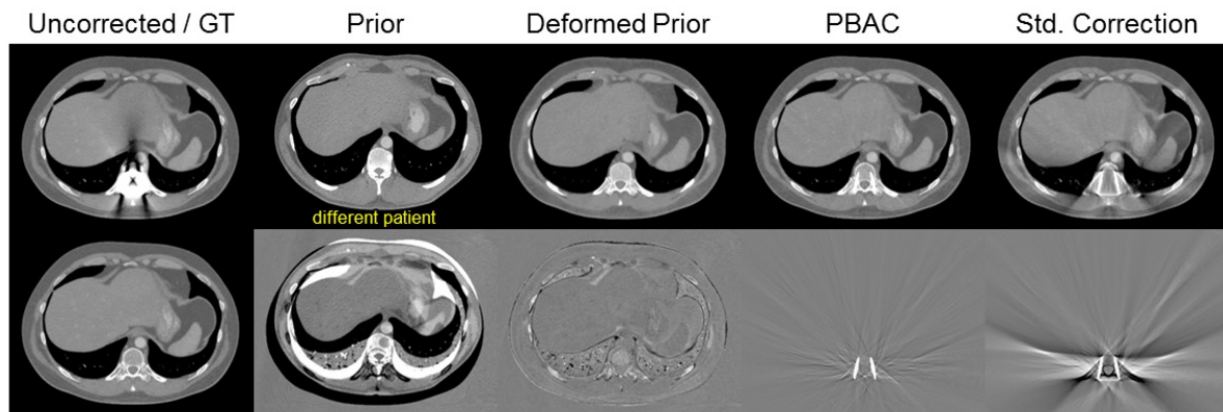


Fig. 6: PBAC results in the metal case. Top row: Uncorrected image, prior used for data completion, deformed prior after registration and the correction result obtained by PBAC. For a comparison, the standard correction is also shown. Bottom row: Ground truth (GT) and the corresponding difference images. $C = 0$ HU, $W = 1000$ HU for reconstructions and for difference images.

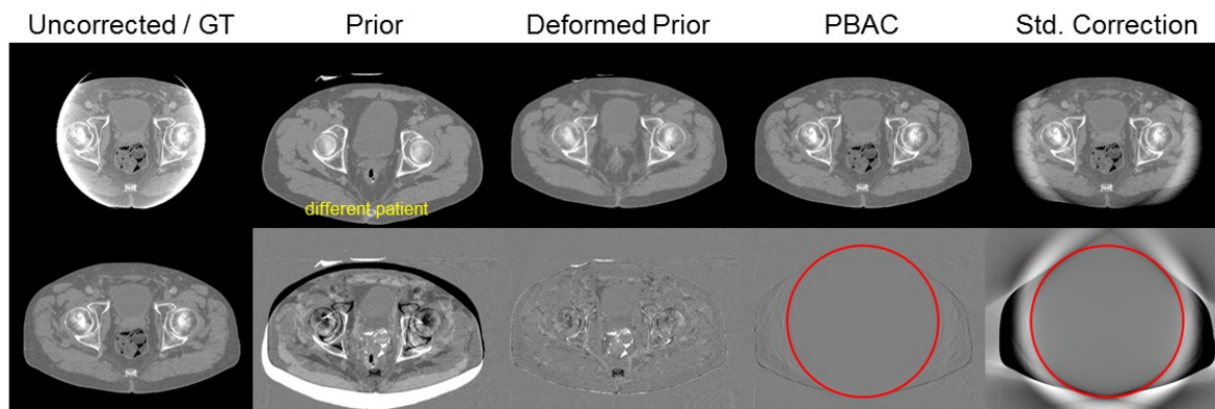


Fig. 7: PBAC results in the truncation case. Top row: Uncorrected image, prior used for data completion, deformed prior after registration and the correction result obtained by PBAC. For a comparison, the standard correction is also shown. Bottom row: Ground truth (GT) and the corresponding difference images. $C = 0$ HU, $W = 1000$ HU for reconstructions and for difference images.

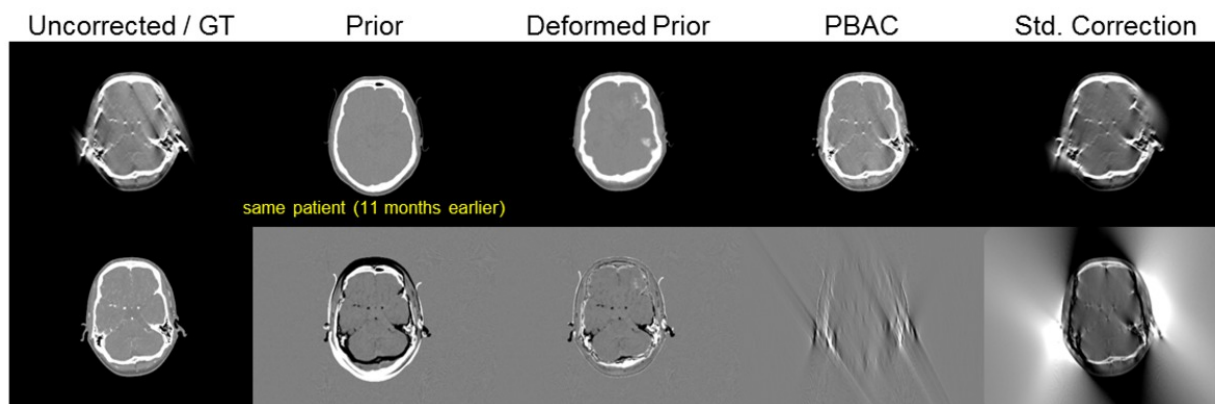


Fig. 8: PBAC results in the limited angle case. Top row: Uncorrected image, prior used for data completion, deformed prior after registration and the correction result obtained by PBAC. For a comparison, the standard correction is also shown. Bottom row: Ground truth (GT) and the corresponding difference images. $C = 0$ HU, $W = 1000$ HU for reconstructions and for difference images.

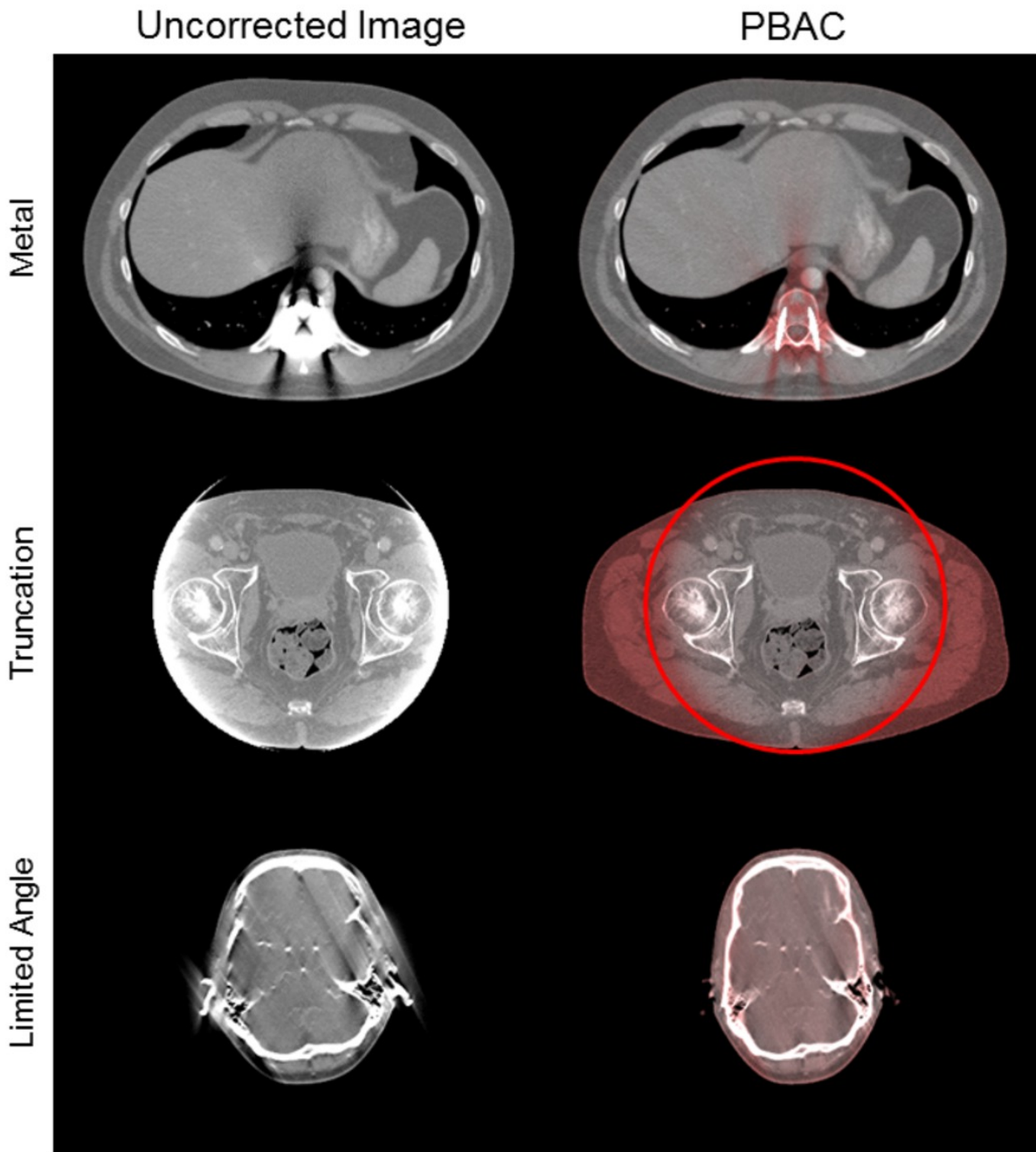


Fig. 9: Uncorrected and corrected images obtained by PBAC. The influence of the prior data is indicated by the red color. $C = 0$ HU, $W = 1000$ HU.

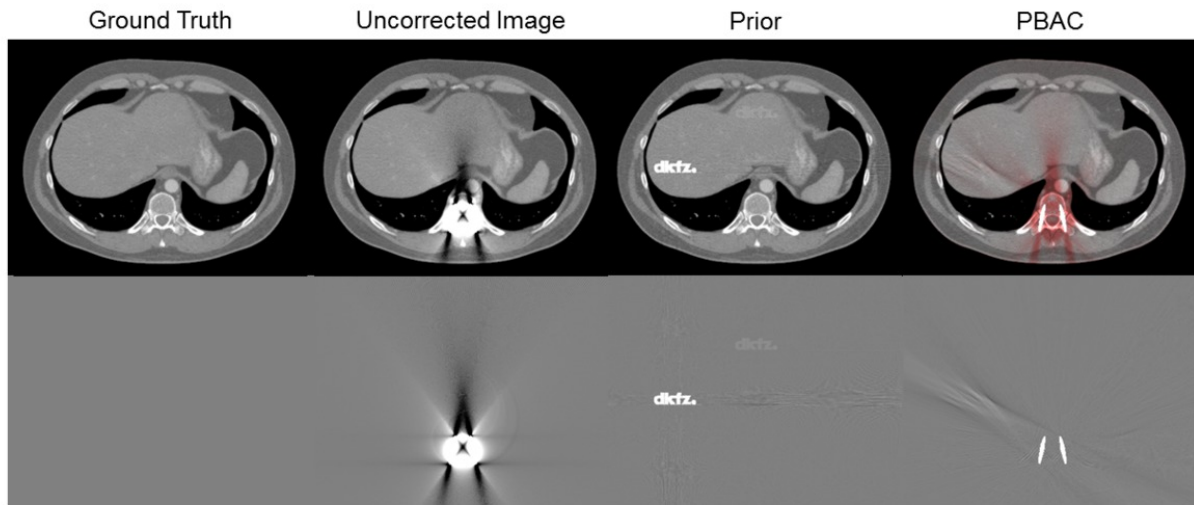


Fig. 10: Thorax patient with metal artifacts and the correction result obtained by performing PBAC using the ground truth including two artificial structures in form of the DKFZ-logo as prior. The difference images show the differences to the ground truth. $C = 0$ HU, $W = 1000$ HU for reconstructions and for difference images.

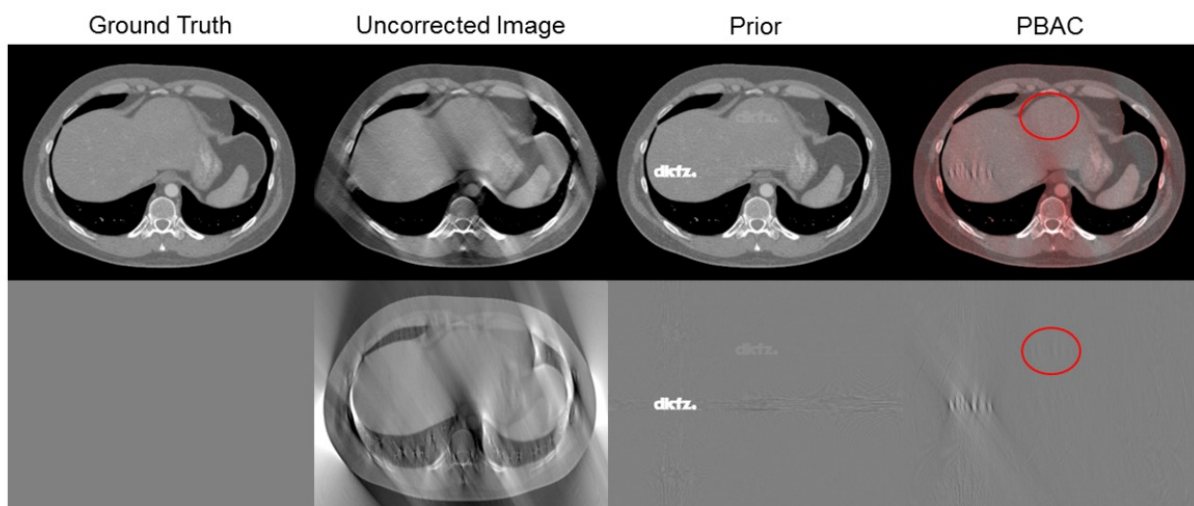


Fig. 11: Thorax patient with limited angle artifacts and the correction result obtained by performing PBAC using the ground truth including two artificial structures in form of the DKFZ-logo as prior. The difference images show the differences to the ground truth. $C = 0$ HU, $W = 1000$ HU for reconstructions and for difference images.

Conclusion

The results obtained so far indicate that the proposed prior-based artifact correction (PBAC) method is able to effectively correct for metal, truncation, and limited angle artifacts. The corrected images are almost artifact-free in the metal and truncation case while some artifacts remain in the corrected images in the limited angle case.

In all cases, PBAC is superior to the conventional data extrapolation or interpolation methods. PBAC comes with a higher artifact suppression while at the same time preserves the patient anatomy in contrast to the conventional methods. It provides better image quality and is therefore better suited for reliable medical diagnosis.

Future research needs to focus on measured instead of simulated artifacts as it is done in this work. Of special interest are experiments where the prior data are acquired with a different imaging modality than the patient data. A realistic scenario would be a patient data set acquired with a flat detector CT, which often results in truncation or limited angle artifacts, and a prior data set measured with a clinical CT. An interesting option may also be the usage of MRI data to perform data completion of a CT data set or vice versa. This leads to particularly interesting solutions for the attenuation correction problem of PET/MRI.

References

- [1] W. A. Kalender, R. Hebel, and J. Ebersberger, "Reduction of CT artifacts caused by metallic implants," *Radiology*, vol. 164, no. 2, pp. 576-577, 1987.
- [2] G. Wang, D. L. Snyder, J. A. O'Sullivan, and M. W. Vannier, "Iterative deblurring for CT metal artifact reduction," *IEEE Transactions on Medical Imaging*, vol. 15, no. 5, pp. 657-664, 1996.
- [3] M. Bal and L. Spies, "Metal artifact reduction in CT using tissue-class modeling and adaptive prefiltering," *Medical Physics*, vol. 33, no. 8, pp. 2852-2859, 2006.
- [4] E. Meyer, R. Raupach, M. Lell, B. Schmidt, and M. Kachelrieß, "Normalized metal artifact reduction (NMAR) in computed tomography," *Medical Physics*, vol. 37, no. 10, pp. 5482-5493, 2010.

- [5] E. Meyer, R. Raupach, M. Lell, B. Schmidt, and M. Kachelrieß, "Frequency split metal artifact reduction (FSMAR) in computed tomography," *Medical Physics*, vol. 39, no. 4, pp. 1904-1916, 2012.
- [6] T. Inouye, "Image reconstruction with limited angle projection data," *IEEE Transactions on Nuclear Science*, vol. 26, no. 2, pp. 2666-2669, 1979.
- [7] S.F. Yau and S.H.Wong, "A linear sinogram extrapolator for limited angle tomography," *3rd International Conference on Signal Processing*, vol. 1, pp. 386-389, 1996.
- [8] L. Ritschl, F. Bergner, and M. Kachelrieß, "A new approach to limited angle tomography using the compressed sensing framework," *Proc.SPIE*, vol. 7622, pp. 76222H, 2010.
- [9] H. Schomberg, "Image reconstruction from truncated cone-beam projections," *IEEE International Symposium on Biomedical Imaging*, pp. 575-578, 2004.
- [10] K. Sourbelle, M. Kachelrieß, and W.A. Kalender, "Reconstruction from truncated projections in CT using adaptive detruncation," *European Radiology*, vol. 15, no. 5, pp. 1008-1014, 2005.
- [11] A. A. Zamyatin and S. Nakanishi, "Extension of the reconstruction field of view and truncation correction using sinogram decomposition," *Medical Physics*, vol. 34, no. 5, pp. 1593-1604, May 2007.
- [12] L. Feldkamp, L. Davis, and J. Kress, "Practical cone-beam algorithm," *Journal of the Optical Society of America*, vol. 1, no. 6, pp. 612-619, 1984.
- [13] C. Maaß, M. Knaup, and M. Kachelrieß, "New approaches to region of interest computed tomography," *Medical Physics*, vol. 38, no. 6, pp. 2868-2878, 2011.
- [14] P. M. Joseph, "An improved algorithm for reprojecting rays through pixel images," *IEEE Transactions on Medical Imaging*, vol. 2, no. 3, pp. 192-196, 1982.
- [15] P. A. Viola and W. M. Wells III, "Alignment by maximization of mutual information," *International Journal of Computer Vision*, vol. 24, no. 2, pp. 137-154, 1997.

[16] C. Studholme, D.L.G. Hill, D.J. Hawkes, et al, "An overlap invariant entropy measure of 3D medical image alignment," *Pattern Recognition*, vol. 32, no. 1, pp. 71-86, 1999.

[17] S. Sawall, M. Knaup, and M. Kachelrieß, "A robust geometry estimation method for spiral, sequential and circular cone-beam micro-CT," *Medical Physics*, vol. 39, no. 9, pp. 5384-5392, 2012.

[18] M. Brehm, P. Paysan, M. Oehlhafen, P. Kunz, and M. Kachelrieß, "Self-adapting cyclic registration for motion-compensated cone-beam CT in image-guided radiation therapy," *Medical Physics*, vol. 39, no. 12, pp. 7603-7618, 2012.

Personal Information

Thorsten Heußner, Marcus Brehm, Dr. Stefan Sawall, and Prof. Dr. Marc Kachelrieß, Medical Physics in Radiology, German Cancer Research Center (DKFZ), Im Neuenheimer Feld 280, 69120 Heidelberg, Germany.

Marcus Brehm, Dr. Stefan Sawall, and Prof. Dr. Marc Kachelrieß, Institute of Medical Physics, Friedrich-Alexander-University (FAU) Erlangen-Nürnberg, Henkestr. 91, 91052 Erlangen, Germany.

Corresponding author: thorsten.heusser@dkfz.de